



Published in final edited form as:

*J Am Chem Soc.* 2017 November 08; 139(44): 15628–15631. doi:10.1021/jacs.7b09790.

## Perfluoroarene–Based Peptide Macrocycles to Enhance Penetration Across the Blood–Brain Barrier

Colin M. Fadzen<sup>†,§</sup>, Justin M. Wolfe<sup>†,§</sup>, Choi-Fong Cho<sup>‡</sup>, E. Antonio Chiocca<sup>‡</sup>, Sean E. Lawler<sup>‡,\*</sup>, and Bradley L. Pentelute<sup>†,\*,iD</sup>

<sup>†</sup>Department of Chemistry, Massachusetts Institute of Technology, Cambridge, Massachusetts 02139, United States

<sup>‡</sup>Harvey Cushing Neuro-Oncology Laboratories, Department of Neurosurgery, Brigham and Women's Hospital, Harvard Medical School, Boston, Massachusetts 02115, United States


### Abstract

Here we describe the utility of peptide macrocyclization through perfluoroaryl-cysteine  $S_NAr$  chemistry to improve the ability of peptides to cross the blood–brain barrier. Multiple macrocyclic analogues of the peptide transportan-10 were investigated that displayed increased uptake in two different cell lines and improved proteolytic stability. One of these analogues (M13) exhibited substantially increased delivery across a cellular spheroid model of the blood–brain barrier. Through *ex vivo* imaging of mouse brains, we demonstrated that this perfluoroarene-based macrocycle of TP10 exhibits increased penetration of the brain parenchyma following intravenous administration in mice. Finally, we evaluated macrocyclic analogues of the BH3 domain of the BIM protein to assess if our approach would be applicable to a peptide of therapeutic interest. We identified a BIM BH3 analogue that showed increased penetration of the brain tissue in mice.

The blood–brain barrier (BBB) poses a significant challenge to delivering therapeutics to the brain, which limits treatment options for central nervous system diseases including primary tumors, brain metastases, autoimmune diseases, and infections.<sup>1</sup> The brain endothelial layer that comprises the BBB is highly specialized, containing continuous tight junctions, a high electrical resistance, and many efflux pumps that extrude drugs from the brain into the blood. Previous efforts to deliver therapeutics across the BBB have focused on temporary chemical or mechanical disruption of the barrier or inhibition of efflux pumps.<sup>2</sup> Both of these techniques have significant limitations. Even when successful in mediating delivery across the BBB, these approaches are nonspecific and thus may also enhance the delivery of unwanted substances into the brain and cause neurotoxicity.<sup>1c</sup>

\*Corresponding Authors, slawler@bwh.harvard.edu, blp@mit.edu.

§C.M.F. and J.M.W. contributed equally.

ORCID 

Bradley L. Pentelute: 0000-0002-7242-801X

Supporting Information

The Supporting Information is available free of charge on the ACS Publications website at DOI: 10.1021/jacs.7b09790.

Full experimental and characterization details (PDF)

The authors declare no competing financial interest.

Significant work to overcome the challenge of specificity has been devoted to molecular delivery vectors, also called “BBB shuttles”.<sup>3</sup> These delivery vectors have classically targeted receptors on the surface of brain endothelial cells, such as the insulin and transferrin receptors.<sup>4</sup> In addition to antibody-based BBB-shuttles, peptide shuttles have shown promise for cargo delivery across the BBB.<sup>5</sup> Peptides are easier to characterize than antibodies and can be prepared by chemical synthesis, enabling the incorporation of diverse chemical moieties to modulate the shuttle’s properties.

Many peptides, however, do not possess an intrinsic ability to cross the BBB and are susceptible to proteolytic degradation. Over the past 25 years, many chemical strategies have been developed for peptide macrocyclization<sup>6</sup> which can confer favorable biological properties to the peptide, such as increased uptake into cells or resistance to proteolysis.<sup>6g,7</sup> We recently reported methodology that allows for the macrocyclization of an unprotected peptide between two cysteine residues with a perfluoroaryl linker through  $S_NAr$  chemistry.<sup>8</sup> We demonstrated that these perfluoroarene-based peptide macrocycles had increased cellular uptake and increased resistance to proteolytic degradation compared with their linear counterparts.

Here we show that our  $S_NAr$  macrocyclization chemistry can be utilized to facilitate peptide crossing of the BBB. We observed that several perfluoroarene-based, macrocyclic analogues of transportan-10 (TP10) have enhanced uptake into two different cell types, including brain endothelial cells. Therefore, we hypothesized that these macrocycles may serve as delivery tools for transport across the BBB. We tested TP10 analogues in a culture-based spheroid model of the BBB that recapitulates many of the important known barrier functions of the BBB. We also tested the top TP10 analogue in mice to demonstrate the applicability of our technology to *in vivo* brain penetration. Finally, we examined the generalizability of this technology to a peptide of therapeutic interest both in the BBB spheres and in mice. This work highlights the potential of perfluoroarene-based peptide macrocycles as brain-penetrating agents.

Our initial experiments were designed to determine the extent to which macrocyclization through our perfluoroaryl-cysteine  $S_NAr$  chemistry could modulate the biological properties of a model peptide known for its ability to translocate across cell membranes.<sup>9</sup> Analogues of this model peptide, TP10, were prepared containing two cysteine residues in a variety of *i, i* +7 configurations (Figure 1). Cysteines were substituted rather than inserted into the sequence in an effort to maintain the spatial relationships between the other amino acids of the peptide. In addition to the macrocyclic aryl variants (denoted M), linear controls (denoted Q\*) were also prepared in which the cysteines were alkylated with 2-bromoacetamide to account for changes in behavior that may arise from the cysteine mutation. To facilitate conjugation of a fluorophore via copper-catalyzed click chemistry, 4-pentynoic acid was coupled to the N-terminus of all peptides.

For our initial experiments, 5-carboxytetramethylrhodamine (5-TAMRA) was conjugated to the N-terminal alkyne of all analogues. To examine these fluorophore-labeled constructs in a biological context, we treated HeLa cells with 2.5  $\mu M$  of each construct for 2 h in serum-free media. After washing with trypsin and buffer to remove any cell surface-adherent peptide,

we observed that all macrocyclic variants of TP10 demonstrated increased mean fluorescence intensity compared with their respective alkyl control by flow cytometry (Figure S1). Encouraged by these results, we sought to determine if this observation was recapitulated in hCMEC/D3 endothelial cells—an immortalized cell line that has been extensively characterized for brain endothelial cell phenotype and is used in models of the BBB.<sup>10</sup> Identical treatment conditions were used except the treatment media for the hCMEC/D3 cells was supplemented with 2% human serum. All macrocyclic variants of TP10 displayed an increase in mean fluorescence intensity with respect to both the native TP10 sequence and their respective alkyl control (Figure 2), indicating increased uptake into hCMEC/D3 cells. Given that brain endothelial cells are a key component of the BBB, we hypothesized that perfluoroarene-based macrocycles may also have increased ability to cross the BBB and accumulate in the brain.

The stability of the macrocyclic TP10 analogues was assayed by incubating 100  $\mu\text{M}$  of each construct with 1.75 nM Proteinase K at 37 °C. After 2 h of incubation with the protease, all macrocyclic variants were still >90% intact, while <40% of the native TP10 remained (Figure S3). Taken with the observation that the linear alkyl controls were no more stable than the native TP10 (Figure S3), these data suggest that the perfluoroarene macrocycle confers beneficial proteolytic stability. Finally, to ensure that the macrocyclic TP10 analogues did not compromise the plasma membrane, a lactate dehydrogenase (LDH) assay was performed using HeLa cells. Neither M13 nor M14 showed appreciable LDH leakage at concentrations of 5  $\mu\text{M}$  or below, indicating that at biologically relevant concentrations, the plasma membrane of the cells was not compromised (Figure S4).

Our next set of experiments was designed to test if our macrocyclic peptides could potentially cross the BBB using the cellular BBB spheroid model.<sup>11</sup> The spheroid model employed in this work consists of a 1:1:1 ratio of human brain microvascular endothelial cells (hCMEC/D3), human brain vascular pericytes (HBVPs), and human astrocytes that spontaneously self-organize into spheres when cocultured. In the brain, the blood vessels are lined with endothelial cells, which associate closely with pericytes and astrocytes to form the BBB.<sup>12</sup> In the spheres, endothelial cells interact with pericytes to line the outermost surface of the sphere, while astrocytes make up the spheroid core (Figure 3). The ability of a molecule to penetrate the surface of the sphere and accumulate in the core represents delivery into the brain. Previous work has shown that these spheres display several of the key properties of the BBB, including high expression of tight junction proteins, upregulation of drug efflux pumps, and receptor-mediated transport across the barrier.<sup>13</sup>

The spheres were treated with 5  $\mu\text{M}$  of each TP10 analogue for 3.5 h at 37 °C. After treatment, the spheres were imaged by confocal microscopy. Quantification of spheroid entry was performed by measuring the mean 5-TAMRA fluorescence intensity at a depth of 90  $\mu\text{m}$  into the core of the spheroid (Figure 3, Figure S6). Of the three macrocyclic analogues, both M13 and M14 displayed increased penetration of the sphere with respect to both native TP10 and their alkyl analogues (Figure S5). M13 showed the greatest increase with an 8-fold change over TP10. These data suggest that both M13 and M14 may have increased ability to cross the BBB. Intriguingly, the location of the perfluoroarene within the

sequence significantly affected the ability of a given analogue to enter the sphere, despite all analogues having increased uptake into brain endothelial cells.

Next, we assessed whether or not the enhanced spheroid penetration we observed could be translated to *in vivo* BBB penetration in a living system. Given the superior influx of M13 into the spheres, M13 was chosen for further evaluation in mice. Cy5.5 was attached to the N-terminal alkyne of M13 and Q\*13. First, 100  $\mu\text{L}$  of a 100  $\mu\text{M}$  solution of each peptide was injected into the tail vein (corresponding to  $\sim 1.5$  mg/kg). After 4 h, the mice were infused intravenously with 50  $\mu\text{L}$  of 50 mg/mL TRITC-dextran, which allows visualization of highly perfused blood vessels. At 4.5 h, the mice were sacrificed. The brain, spleen, kidneys, lungs, heart, and liver were excised, flash frozen, and imaged on an *in vivo* imaging system (IVIS) (Figure 4A, Figures S13 and S14). The total radiant efficiency from Cy5.5 in each organ was quantified (Figure S12). The liver and kidneys were brightest for both M13 and Q\*13, although the amount of signal was similar between the macrocycle and control. However, in the brains of mice treated with the macrocycle, the total radiant efficiency was over double that of the linear control, suggesting increased uptake of the macrocycle into the brain.

Given the resolution of the IVIS instrument, distinguishing fluorescence in the actual brain tissue from fluorescence in the blood vessels of the brain can be challenging. Therefore, we performed a more detailed analysis by *ex vivo* brain imaging using high-resolution confocal microscopy to confirm the peptide was actually entering the brain parenchyma. The frozen brains were cryosectioned into 30  $\mu\text{m}$  slices after IVIS imaging, and the slices were imaged by confocal microscopy. M13 can be observed outside of the vessel and in the brain parenchyma, providing evidence that the macrocyclic peptide is crossing the BBB and entering the brain tissue (Figure 4B,C). Additionally, a serum stability assay was performed by incubating each peptide in 5% mouse serum and measuring degradation over 24 h (Figure S9). M13 displayed greater serum stability, suggesting that the increase in brain penetration is likely due to both increased stability in serum and increased ability to cross the BBB.

Finally, we wanted to see if our findings could be generalized to a peptide of therapeutic interest. We chose the BH3 domain of the pro-apoptotic BIM protein, as Bird *et al.* have conducted an exhaustive staple scan of the peptide and demonstrated which positions are amenable to mutation.<sup>14</sup> We synthesized two BIM BH3 peptide sequences but substituted cysteine residues for the  $\alpha,\alpha$ -disubstituted olefin-bearing amino acids previously employed (Figure 5A). To evaluate the ability of our perfluoroarene-based macrocyclic BIM BH3 variants to cross the BBB, we performed the same sequence of experiments under the same conditions as we did with TP10. First, TAMRA-labeled BIM BH3 analogues were tested in BBB spheres. BIM M4 had significantly increased fluorescence in the core of the sphere, compared to both its linear alkyl control and to a hydrocarboncyclized control (Figure 5B, Figures S7 and S8). Conversely, although bright on the sphere surface, M9 had little fluorescence in the sphere core. As a result, we carried Cy5.5-BIM M4 and its alkyl control Cy5.5-BIM Q\*4 forward for *in vivo* evaluation. The perfluoroarene macrocycle had a modest increase in total radiant efficiency in the brain by IVIS relative to the alkyl control (Figure 5C, Figures S12 and S14). When the brain was sectioned and imaged by confocal microscopy, significantly more Cy5.5 fluorescence was observed in the brain parenchyma for BIM M4 than BIM Q\*4 (Figure 5D,E, Figure S17). Altogether, these data suggest that

the perfluoroarene macrocycle improves the ability of the BIM BH3 peptide to cross the BBB.

In conclusion, we have demonstrated with our proof-of-concept experiments that abiotic peptide macrocycles can exhibit significantly enhanced penetration of the brain. While synthetic peptide macrocycles have been engineered as successful inhibitors of protein–protein interactions, especially for cancer therapeutics, they are just starting to be explored for crossing the BBB.<sup>14</sup> Here we show the first example of improving brain penetration solely through the introduction of an abiotic macrocycle. The mechanism of transport across the BBB and the role of linker placement remain to be elucidated. However, given the widespread interest in peptide macrocyclization, we expect this finding may be of immediate use to the scientific community in designing therapeutics and imaging agents for central nervous system diseases.

## Supplementary Material

Refer to Web version on PubMed Central for supplementary material.

## Acknowledgments

This work was supported by the National Institutes of Health (NIH; R01GM110535) and the Sontag Foundation Distinguished Scientist Award (to B.L.P.) C.M.F. is supported by the David H. Koch Graduate Fellowship Fund. J.M.W. is supported by the National Science Foundation Graduate Research Fellowship under Grant No. 1122374. C.-F.C. is supported by the Canadian Institute of Health Research Fellowship. We acknowledge the Swanson Biotechnology Center Flow Cytometry Facility at the Koch Institute for the use of their flow cytometers, IVIS instrumentation, and advice. We also acknowledge Yarah Ghotmi for assistance in brain cryosections, Roscoe Wasserburg for assistance with tissue culture, and Alex Mijalis for assistance in the synthesis of the hydrocarbon-stapled peptide.

## References

1. (a) Deeken JF, Löscher W. *Clin. Cancer Res.* 2007; 13(6):1663–1674. [PubMed: 17363519] (b) Calvo P, Gouritin B, Villarroja H, Eclancher F, Giannavola C, Klein C, Andreux JP, Couvreur P. *Eur. J. Neurosci.* 2002; 15(8):1317–1326. [PubMed: 11994126] (c) Chen Y, Liu L. *Adv. Drug Delivery Rev.* 2012; 64(7):640–665. (d) Nau R, Sörgel F, Eiffert H. *Clin. Microbiol. Rev.* 2010; 23(4):858–883. [PubMed: 20930076]
2. (a) Löscher W, Potschka H. *Nat. Rev. Neurosci.* 2005; 6(8):591–602. [PubMed: 16025095] (b) Abbott NJ, Revest PA. *Cerebrovasc. Brain Metab. Rev.* 1991; 3(1):39–72. [PubMed: 2036300] (c) Sanovich E, Bartus RT, Friden PM, Dean RL, Le HQ, Brightman MW. *Brain Res.* 1995; 705(1–2): 125–135. [PubMed: 8821743] (d) Sheikov N, McDannold N, Vykhodtseva N, Jolesz F, Hynynen K. *Ultrasound Med. Biol.* 2004; 30(7):979–989. [PubMed: 15313330]
3. Oller-Salvia B, Sánchez-Navarro M, Giralt E, Teixidó M. *Chem. Soc. Rev.* 2016; 45(17):4690–4707. [PubMed: 27188322]
4. (a) Kumagai AK, Eisenberg JB, Pardridge WM. *J. Biol. Chem.* 1987; 262(31):15214–15219. [PubMed: 2959663] (b) Friden PM, Walus LR, Musso GF, Taylor MA, Malfroy B, Starzyk RM. *Proc. Natl. Acad. Sci. U. S. A.* 1991; 88(11):4771–4775. [PubMed: 2052557]
5. (a) Schwarze SR, Ho A, Vocero-Akbani A, Dowdy SF. *Science.* 1999; 285(5433):1569–1572. [PubMed: 10477521] (b) Kumar P, Wu H, McBride JL, Jung K-E, Hee Kim M, Davidson BL, Kyung Lee S, Shankar P, Manjunath N. *Nature.* 2007; 448(7149):39–43. [PubMed: 17572664] (c) Oller-Salvia B, Sánchez-Navarro M, Ciudad S, Guiu M, Arranz-Gibert P, Garcia C, Gomis RR, Cecchelli R, García J, Giralt E, Teixidó M. *Angew. Chem. Int. Ed.* 2016; 55(2):572–575.
6. (a) Brown SP, Smith AB. *J. Am. Chem. Soc.* 2015; 137(12):4034–4037. [PubMed: 25793939] (b) Kalhor-Monfared S, Jafari MR, Patterson JT, Kitov PI, Dwyer JJ, Nuss JM, Derda R. *Chem. Sci.*

- 2016; 7(6):3785–3790.(c) Schafmeister CE, Po J, Verdine GL. *J. Am. Chem. Soc.* 2000; 122(24): 5891–5892.(d) Blackwell HE, Grubbs RH. *Angew. Chem. Int. Ed.* 1998; 37(23):3281–3284.(e) Botti P, Pallin TD, Tam JP. *J. Am. Chem. Soc.* 1996; 118(42):10018–10024.(f) Lau YH, de Andrade P, McKenzie GJ, Venkitaraman AR, Spring DR. *ChemBioChem.* 2014; 15(18):2680–2683. [PubMed: 25354189] (g) White CJ, Yudin AK. *Nat. Chem.* 2011; 3(7):509–524. [PubMed: 21697871]
7. (a) Walensky LD, Kung AL, Escher I, Malia TJ, Barbuto S, Wright RD, Wagner G, Verdine GL, Korsmeyer SJ. *Science.* 2004; 305(5689):1466–1470. [PubMed: 15353804] (b) Chang YS, Graves B, Guerlavais V, Tovar C, Packman K, To K-H, Olson KA, Kesavan K, Gangurde P, Mukherjee A, Baker T, Darlak K, Elkin C, Filipovic Z, Qureshi FZ, Cai H, Berry P, Feyfant E, Shi XE, Horstick J, Annis DA, Manning AM, Fotouhi N, Nash H, Vassilev LT, Sawyer TK. *Proc. Natl. Acad. Sci. U. S. A.* 2013; 110(36):E3445–E3454. [PubMed: 23946421] (c) Lautrette G, Touti F, Lee HG, Dai P, Pentelute BL. *J. Am. Chem. Soc.* 2016; 138(27):8340–8343. [PubMed: 27332147] (d) Grossmann TN, Yeh JT-H, Bowman BR, Chu Q, Moellering RE, Verdine GL. *Proc. Natl. Acad. Sci. U. S. A.* 2012; 109(44):17942–17947. [PubMed: 23071338]
8. (a) Spokoyny AM, Zou Y, Ling JJ, Yu H, Lin Y-S, Pentelute BL. *J. Am. Chem. Soc.* 2013; 135(16): 5946–5949. [PubMed: 23560559] (b) Zou Y, Spokoyny AM, Zhang C, Simon MD, Yu H, Lin Y-S, Pentelute BL. *Org. Biomol. Chem.* 2014; 12(4):566–573. [PubMed: 24310320]
9. (a) Islam MZ, Ariyama H, Alam JM, Yamazaki M. *Biochemistry.* 2014; 53(2):386–396. [PubMed: 24397335] (b) Fanghänel S, Wadhvani P, Strandberg E, Verdurmen WPR, Bürck J, Ehni S, Mykhailiuk PK, Afonin S, Gerthsen D, Komarov IV, Brock R, Ulrich AS. *PLoS One.* 2014; 9(6):e99653. [PubMed: 24937132]
10. (a) Weksler BB, Subileau EA, Perrière N, Charneau P, Holloway K, Leveque M, Tricoire-Leignel H, Nicotra A, Bourdoulous S, Turowski P, Male DK, Roux F, Greenwood J, Romero IA, Couraud PO. *FASEB J.* 2005; doi: 10.1096/fj.04-3458fje(b) Vu K, Weksler B, Romero I, Couraud P-O, Gelli A. *Eukaryotic Cell.* 2009; 8(11):1803–1807. [PubMed: 19767445]
11. Urich E, Patsch C, Aigner S, Graf M, Iacone R, Freskgård P-O. *Sci. Rep.* 2013; doi: 10.1038/srep01500
12. Abbott NJ, Rönnbäck L, Hansson E. *Nat. Rev. Neurosci.* 2006; 7(1):41–53. [PubMed: 16371949]
13. Cho C-F, Wolfe JM, Fadzen CM, Calligaris D, Hornburg K, Chiocca EA, Agar NYR, Pentelute BL, Lawler SE. *Nat. Commun.* 2017; 8:15623. [PubMed: 28585535]
14. Bird GH, Mazzola E, Opoku-Nsiah K, Lammert MA, Godes M, Neuberg DS, Walensky LD. *Nat. Chem. Biol.* 2016; 12(10):845–852. [PubMed: 27547919]

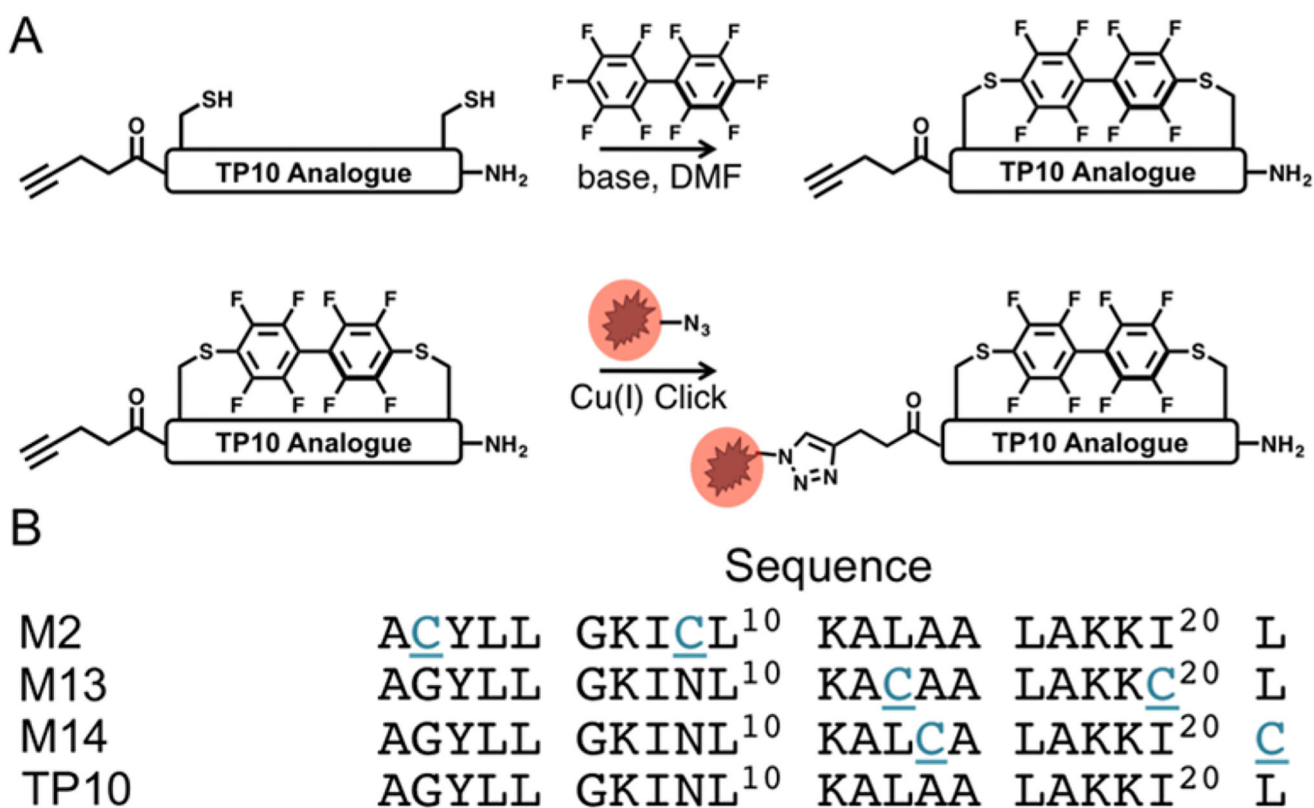


**Figure 1.** Macrocyclic TP10 Analogues prepared via  $S_NAr$ . (A) Workflow for generating fluorophore-containing perfluoroarene-based macrocyclic TP10 analogues. (B) Peptide sequences for the TP10 macrocycles. The N-terminus is capped with 4-pentynoic acid to provide a click handle for labeling.

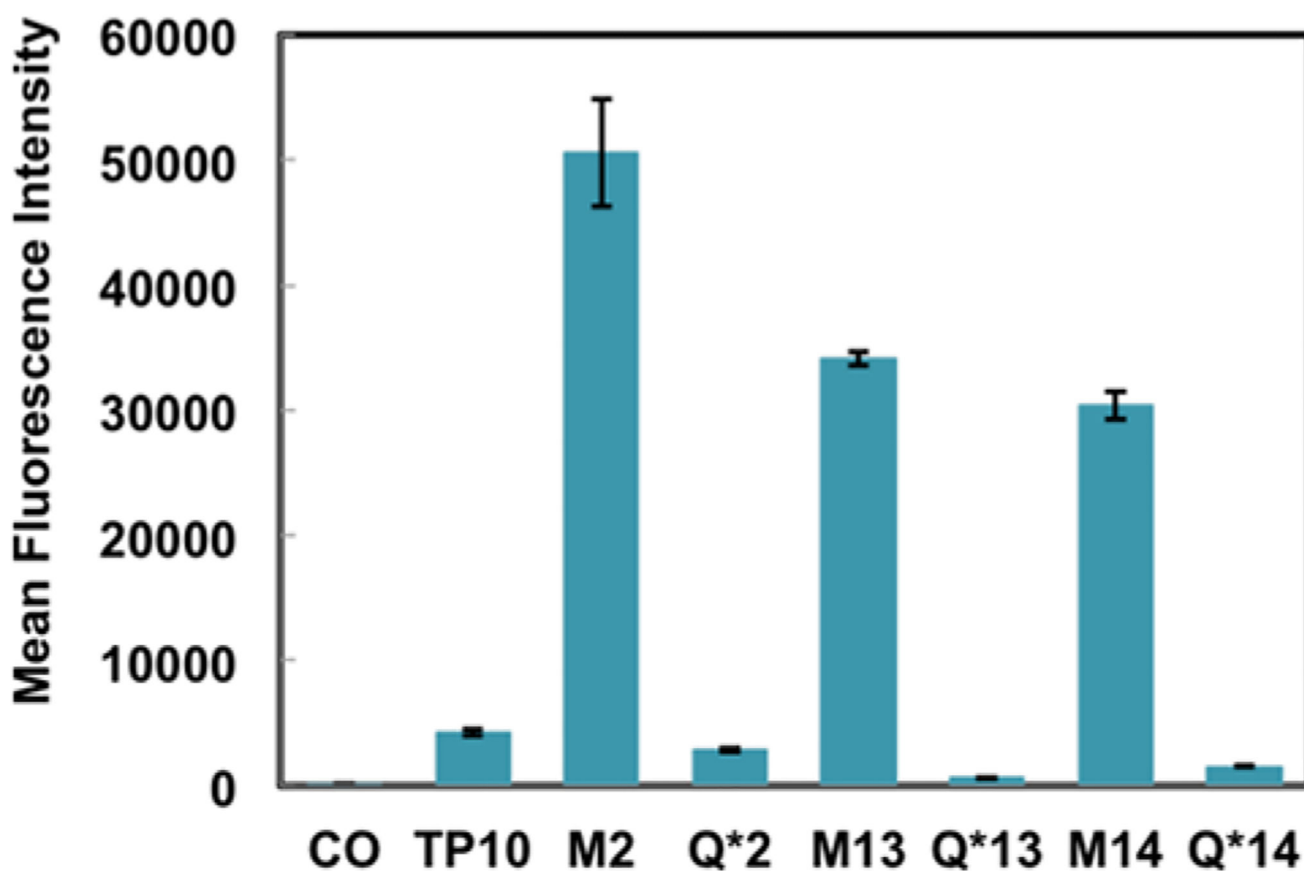


**Figure 2.** Perfluoroarene-based macrocyclic TP10 analogues have increased uptake in endothelial cells. Flow cytometry analysis of hCMEC/D3 cells treated with 2.5  $\mu$ M of each peptide for 2 h at 37  $^{\circ}$ C. The macrocyclic variants display up to a 12-fold increase in mean fluorescence intensity relative to native TP10 ( $n = 3$ ).



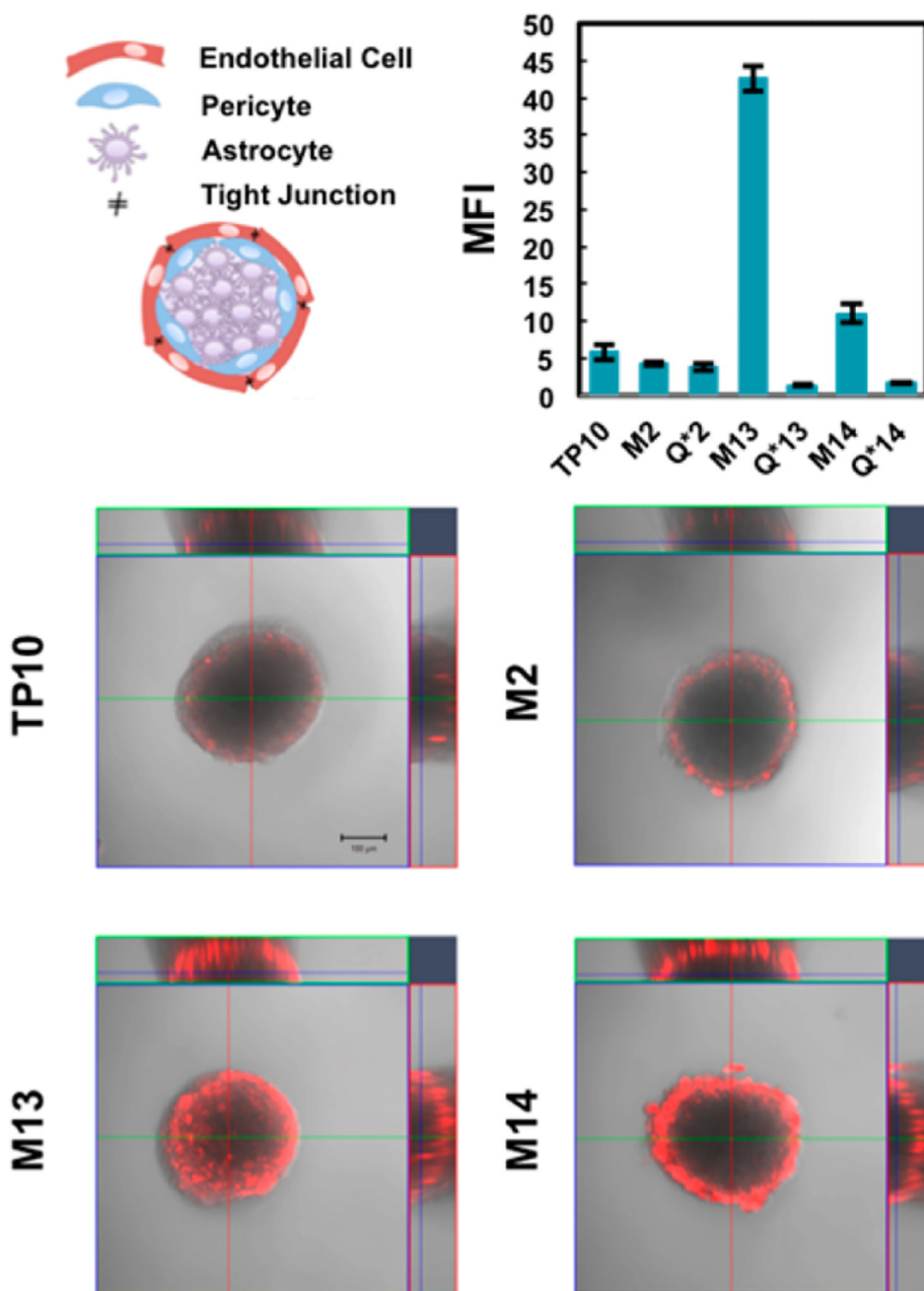


**Figure 3.** Perfluoroarene-based macrocyclic TP10 analogues display increased entry into BBB spheroids compared to their linear counterparts. Schematic illustrating the cellular composition of the spheres (not to scale). The confocal microscopy images display a representative spheroid after incubation with 5  $\mu\text{M}$  of each construct showing an overlay of both fluorescence (5-TAMRA) and brightfield (scale bar = 100  $\mu\text{m}$ ). The images are at a  $z$ -depth of 90  $\mu\text{m}$  into the core of the sphere. The plot shows the mean fluorescence intensity of a 100  $\mu\text{m}$  diameter circular region that excludes fluorescence on the spheroid exterior ( $n = 3-5$ ). For images of the spheres treated with the alkyl controls, see Figure S5.

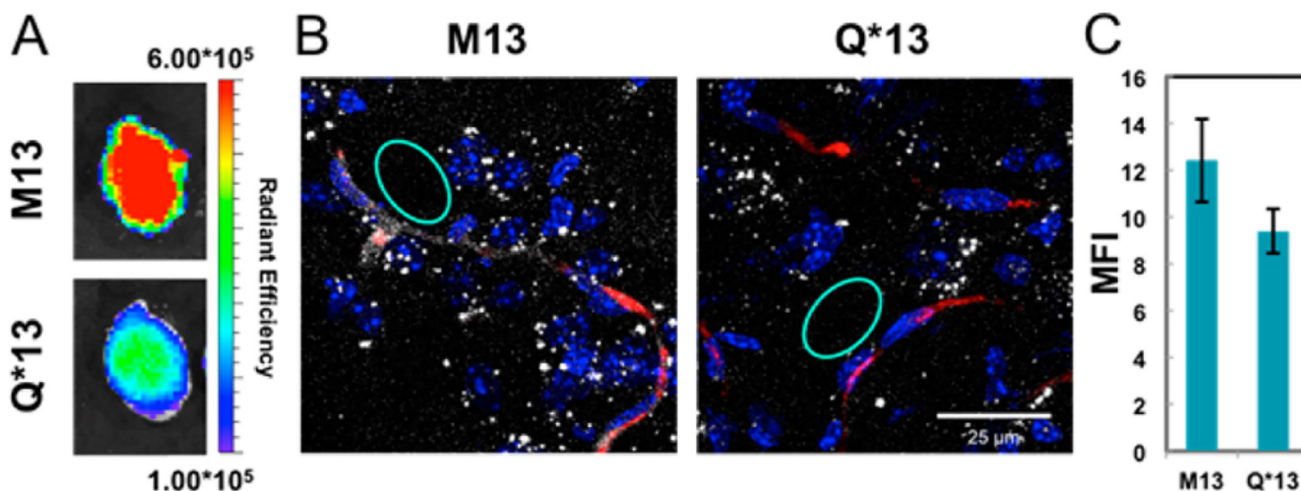


**Figure 4.** Enhanced *in vivo* brain penetration of a perfluoroarene-based TP10 macrocycle. (A) IVIS imaging of mouse brains treated with Cy5.5-labeled TP10 analogues. One representative brain in each group after excitation at 640 nm ( $n = 2$ ). (B) Confocal microscopy images of brain cryosections showing a square area surrounding a capillary. For full confocal images, see Figure S16 (nuclei–Hoechst, blue; dextran–TRITC, red; peptide–Cy5.5, white). (C) Quantification of the diffuse Cy5.5 signal in the brain parenchyma from the confocal images, suggesting accumulation of the TP10 analogues in the brain. The quantification was performed by selecting regions (such as the cyan circles) outside the vessels that did not contain bright puncta and averaging the mean fluorescence intensities from each region ( $n = 10$ ). M13 had a statistically significant increase in mean fluorescence intensity compared with Q\*13 by a Student’s *t*-test ( $P < 0.001$ ).

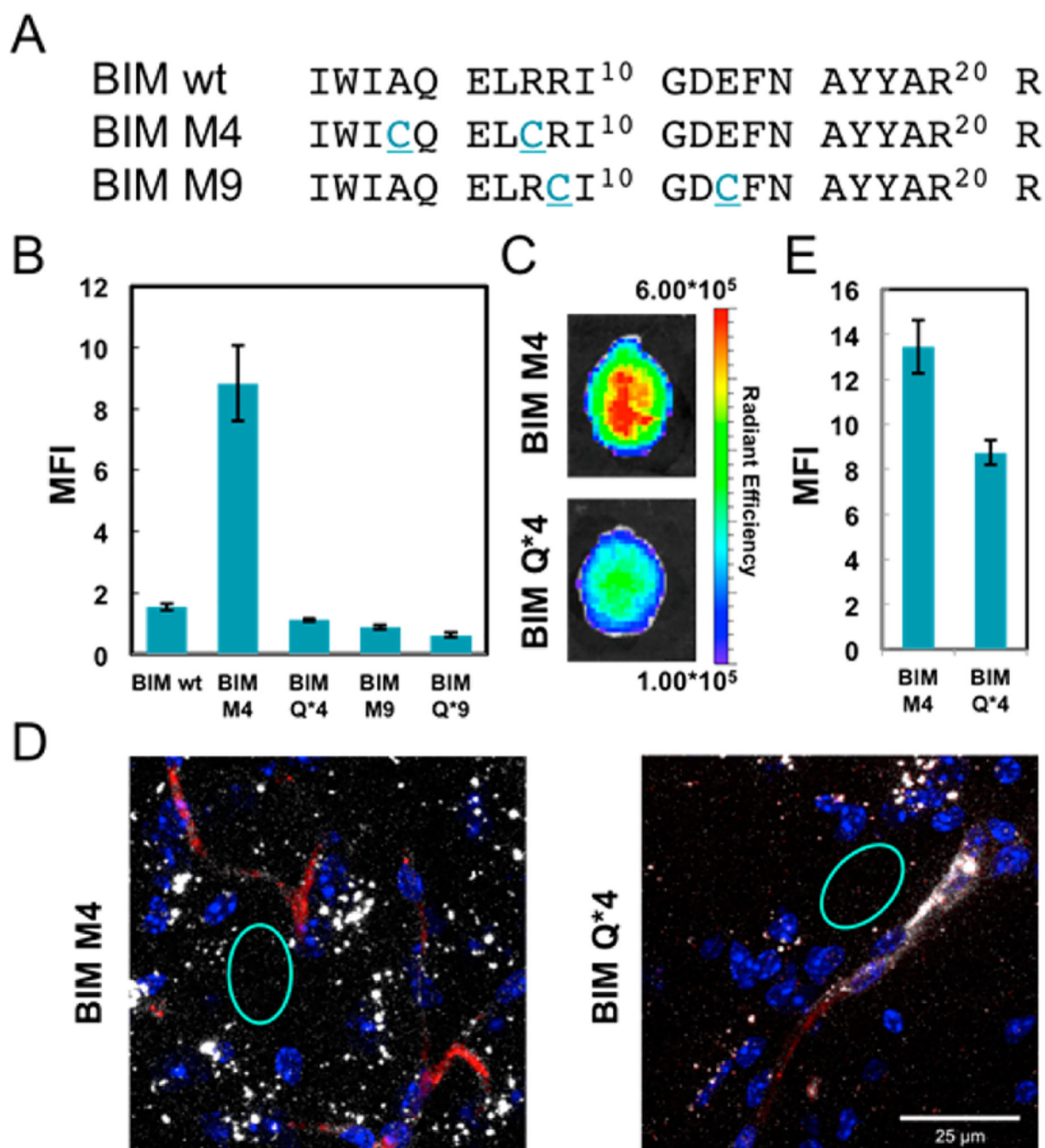


**Figure 5.** Enhanced *in vivo* brain penetration of a perfluoroarene-based BIM BH3 macrocycle. (A) Sequences of the BIM BH3 analogues. (B) Plot of the mean fluorescence intensity in the core of the sphere for TAMRA-labeled BIM BH3 analogues ( $n = 6$ ). (C) IVIS imaging of mouse brains treated with Cy5.5-labeled analogues. One representative brain in each group after excitation at 640 nm ( $n = 2$ ). (D) Confocal microscopy images of brain cryosections showing a square area around a capillary. For full confocal images, see Figure S17 (nuclei–Hoechst, blue, dextran–TRITC, red, peptide–Cy5.5, white). (E) Quantification of the diffuse Cy5.5 signal in the brain parenchyma from the confocal images, suggesting accumulation of

the BIM BH3 analogues in the brain. The quantification was performed by selecting regions (such as the cyan circles) outside the vessels that did not contain bright puncta and averaging the mean fluorescence intensities from each region ( $n = 10$ ). BIM M4 had a statistically significant increase in mean fluorescence intensity compared with BIM Q\*4 by a Student's  $t$  test ( $P < 0.0001$ ).

Author Manuscript

Author Manuscript

Author Manuscript

Author Manuscript